Parisian conurbation and then allows us to study the influence of time travel (about thirty hours from Andrésy taking into account the flow rate of the Seine river during the sampling campaign) on modification of physico-chemical properties of DOM.

The DOM from all these sites has been exhaustively extracted and fractionated according to its polarity into three different fractions: hydrophobic, transphilic and hydrophilic. All details of the procedure are described in (Pernet-Coudrier et al., 2008;Pernet-Coudrier et al., 2010). Briefly, surface water was in-line filtered through subsequent 10 and 0.45-µm polypropylene filters, softened on a cationic exchange resin and concentrated using a field reverse osmosis device. The concentrate was then passed through DAX-8 and XAD-4 resin columns to obtain the HPO and TPI fractions, respectively. The HPI, i.e. the fraction of DOM not retained by DAX-8 and XAD-4 resins, was separated from the inorganic salts by means of zeotrophic distillation, successive salt precipitation and salt trapping on cationic exchange resin. Finally, the eluates were freeze-dried and stored for later use. These fractions have been characterised by elemental analysis, Py-GC-MS, fluorescence, SUVA, FTIR, size exclusion chromatography and ^{13}C and ^{15}N isotopic analysis, see (Filella et al., 2009;Pernet-Coudrier, 2008;Pernet-Coudrier et al., 2010).

Table reports the elemental characterization of the different fractions and shows the efficiency of the procedure to isolate DOM from inorganic salts (Pernet-Coudrier, 2008;Pernet-Coudrier et al., 2010).

2.2 Proton Binding by DOM Fractions

The acid-base properties of the fractions referred to above were studied by proton titrations performed using a computer-controlled titrimeter (2 Titrino 785 DMP, Metrohm) under nitrogen (99.99%) bubbling in a thermostated reaction vessel (25.0°C).

177 The pH was read using a pH Metrohm electrode and an Ag/AgCl glass reference
178 Metrohm electrode with a salt bridge (same concentration as the sample solution: 0.1
179 mol L^{-1} or 0.05 mol L^{-1}). The pH electrode was calibrated by titration with a standard
180 acid solution (0.1 mol L^{-1}, Titrisol) and a standard base solution (CO_2-free KOH, 0.1
181 mol L^{-1} Titrisol) containing the same salt level as the sample solution and fitting the
182 results to a Nernst-type equation. To ensure a complete dissolution of the DOM extracts
183 before the titrations, DOM solutions were maintained at pH 10 for 3 hours, and then
184 stabilised for 1 hour at pH 3. The titration of each DOM fraction with standard KOH
185 was performed at KNO_3 0.1 mol L^{-1} and 0.05 mol L^{-1}. After each acid or base addition,
186 the drift rate of the electrode was measured over 300 s; readings were accepted
187 whenever the drift was less than 0.5 mV min^{-1}.
188 The amount of deprotonated sites (Q, in mol kg^{-1}) of the fractions HPOAN, HPOMT,
189 HPOA1 and TPIA1 can be computed from the charge balance:

190 $$Q = \frac{c_{K^+} + c_{H^+} - c_{NO_3^-} - c_{OH^-}}{c_{DOM}} \quad (2)$$

191 which was evaluated following the standard procedure based on the determination of the
192 initial charge (Q^0) from the initial pH_0 (see eqn. (15) in ref. (Companys et al., 2007a)).
193
194 For HPIA1, a specific treatment is required. Given that pH_o equals 7.2, there must be
195 "basic" sites acting in this fraction. The sites available for protonation or complexation
196 can be classified according to their charge before protonation as negative (labelled "S^{-}",
197 e.g. carboxylic and phenolic **S**ites) or **N**eutral (labelled "N", e.g. sites associated to
198 groups containing Nitrogen). So, the acid-base equilibria are

199 $$-S^- + H^+ \rightleftharpoons -SH \quad (3)$$

200 and

201 $$\text{-N} + \text{H}^+ \rightleftharpoons \text{-NH}^+ \quad (4)$$

202

203 The concentration (in mol kg^{-1}) of sites available for complexation will be

204 $$Q = \left(\left[\text{-S}^- \right] + \left[\text{-N} \right] \right) / c_{\text{DOM}} \quad (5)$$

205

206 The total concentration (in mol L^{-1}) of sites of type **N** (free or protonated) is

207 $$Q'_{\text{max,Neutral}} = \left[\text{-N} \right] + \left[\text{-N}^+ \right] \quad (6)$$

208

209 The charge balance at any point of the titration requires

210 $$c_{\text{K}^+} + c_{\text{H}^+} + \left[\text{-N}^+ \right] = \left[\text{-S}^- \right] + c_{\text{NO}_3^-} + c_{\text{OH}^-} \quad 7)$$

211 Next, by combining eqn. (6) and 7), we obtain the concentration of non-protonated sites
212 in a given point of the protonation curve as

213 $$Q = \frac{\left[\text{-S}^- \right] + \left[\text{-N} \right]}{c_{\text{DOM}}} = \frac{c_{\text{K}^+} + c_{\text{H}^+} + Q'_{\text{max,Neutral}} - c_{\text{NO}_3^-} - c_{\text{OH}^-}}{c_{\text{DOM}}} \quad (8)$$

214 which can be seen as an extension of eqn. (2).

215

216 2.3 Pb Binding by DOM Fractions and AGNES methodology

217

218 Voltammetric measurements were carried out with an Eco Chemie Autolab PGSTAT12
219 potentiostat attached to a Metrohm 663VA Stand, being controlled from a computer by
220 means of the GPES (Eco Chemie) software package. The working electrode was a
221 Metrohm multimode mercury drop electrode (radius of the mercury drop used around
222 1.41×10^{-4} m). The auxiliary electrode was a glassy carbon electrode and the reference
223 electrode was Ag/AgCl/3 mol L^{-1} KCl, with a 0.1 mol L^{-1} KNO_3. A Teflon cell
224 (Metrohm) was thermostated at 25.0 °C by means of a glass jacket connected to a bath.

The pH was monitored with a glass combined electrode (Orion 9103) attached to a pH-meter Basic 20 (Crison).

As it has been already recommended (Town and Filella, 2002), assessment of Pb binding to DOM should be done at the relevant pH and low DOM concentration in order to avoid any artefacts and underestimation of binding parameters. In consequence metal titrations were performed at fixed pH (from 5 to 9) for an initial pre-dissolved DOM concentration of 20 mg L^{-1} in KNO_3 0.1 mol L^{-1} as background electrolyte, by adding standard Pb (1000 mg L^{-1}) solution (Merck), or diluted solutions prepared from this one. The pH was set at the desired value by small additions of KOH and HNO_3 when necessary, and, then, the free Pb concentration was measured with AGNES which has been previously used to study the complexation of Cd, Zn and Pb to humic acids (Companys et al., 2007b;Domingos R.F. et al., 2008;Puy et al., 2008). The principles of AGNES (see details in (Galceran et al., 2004)) are: i) The aim of the first (or deposition) stage is to attain the equilibrium given by eqn 42 with a flat concentration profile for Pb^o. ii) The aim of the second (stripping) stage is the quantification of c_{Pb^o}. When the previous two aims have been achieved, there is a direct proportionality between the measured faradaic current (or charge) and the free Pb^{2+} concentration. In this work, the faradaic current has been computed by subtracting the "shifted" blank current (I_{sb}) (Galceran et al., 2007).

An optimized way of achieving aim i) consists in the two potential strategy (Companys et al., 2005): the application of a potential $E_{1,a}$ (corresponding to a gain $Y_{1,a}>>Y$, under diffusion limited condition for reduction) which enhances the metal deposition during a time t_{1a}, followed by a potential $E_{1,b}$ (corresponding to a gain $Y=Y_{1,b}$, which is the desired gain for the measure) during a time $t_{1,b}$, see Table 2.

The application of AGNES requires the selection of appropriate values for the parameters (gains and times). In this work, we have systematised this selection procedure in the two potential strategy, especially at the lowest metal concentrations as detailed in Fig . The first value of the gain Y (desired relationship between c_{Pb^0} and $c_{Pb} \equiv c_{Pb^{2+}}$ prescribed via the applied potential) at the lowest total Pb concentration, $c_{T,Pb}$, has to be adjusted to yield a current above the limit of detection. An iterative procedure starts with the application of an initial Y and t_{1a}. If the current obtained (with $t_{1,b}$=50 s) is sufficiently different from the blank current (I_{sb}), Y is suitable, otherwise, Y is increased. Once the selected Y is high enough, t_{1a} is optimized, avoiding large overshoots or undershoots (Companys et al., 2005). Notice, following Fig , that t_{1b} is kept short until t_{1a} is sufficiently optimised. After some metal additions, c_{Pb} increases and the value of Y can be progressively reduced, thus reducing the deposition times. For smaller Y, the simplest strategy of one potential pulse is used (Galceran et al., 2004).

The lead bound to the organic matter is obtained by subtracting from the total Pb added, both, the free Pb (measured by AGNES) and the Pb bound to inorganic species ($Pb(NO_3)_2$, $PbNO_3^+$, $PbOH^+$, $Pb(OH)_2$, $Pb(OH)_3^-$), computed using the constants (NIST 46.6) in VMINTEQ (Gustafsson, 2000).

3. THEORETICAL BACKGROUND

3.1 Pb Binding to DOM Fraction

Binding isotherms are equilibrium expressions relating the coverage (θ) to the free metal ion concentration (denoted as c_H or c_{Pb} hereafter). The non-ideal competitive

isotherm (NICA) has been very successful in fitting ion binding to different fractions of organic matter (Kinniburgh et al., 1999;Koopal et al., 1994;van Riemsdijk et al., 1986). Usually, two modal distributions (e.g. associating "1" with "carboxylic" groups and "2" with "phenolic" sites) are suitable, but in this work, a third distribution (e.g. "nitrogen" groups or "neutral" sites) will be added for the fraction HPIA1, given the triple wave shape of the corresponding proton titration (see section 4.2 below). For each modal distribution (denoted with the index *j*), NICA reads:

$$\theta_{\mathrm{Pb},j}\left(c_{\mathrm{H}},c_{\mathrm{Pb}}\right)=\frac{\left(\bar{k}_{\mathrm{Pb},j}c_{\mathrm{Pb}}\right)^{n_{\mathrm{Pb},j}}}{\left(\bar{k}_{\mathrm{H},j}c_{\mathrm{H}}\right)^{n_{\mathrm{H},1}}+\left(\bar{k}_{\mathrm{Pb},j}c_{\mathrm{Pb}}\right)^{n_{\mathrm{Pb},j}}}\frac{\left(\left(\bar{k}_{\mathrm{H},j}c_{\mathrm{H}}\right)^{n_{\mathrm{H},j}}+\left(\bar{k}_{\mathrm{Pb},j}c_{\mathrm{Pb}}\right)^{n_{\mathrm{Pb},j}}\right)^{p_j}}{1+\left(\left(\bar{k}_{\mathrm{H},j}c_{\mathrm{H}}\right)^{n_{\mathrm{H},j}}+\left(\bar{k}_{\mathrm{Pb},j}c_{\mathrm{Pb}}\right)^{n_{\mathrm{Pb},j}}\right)^{p_j}} \tag{9}$$

where $n_{\mathrm{X},j}$ ($0 < n_{\mathrm{X},j} \leq 1$) is a parameter related to the stoichiometric factor of each ion X, p_j ($0 < p_j \leq 1$) is the generic heterogeneity parameter of the macromolecule, and $\bar{k}_{\mathrm{H},j}$ and $\bar{k}_{\mathrm{Pb},j}$ are adsorption parameters related to the strength of each ion binding. The total loading of Pb (in mol kg^{-1}) can be computed as

$$Q_{\mathrm{Pb}}=\sum_{j=1}^{2\,or\,3}\frac{n_{\mathrm{Pb},j}}{n_{\mathrm{H},j}}Q_{\mathrm{max},j}\theta_{\mathrm{Pb},j}=\sum_{j=1}^{2\,or\,3}Q_{\mathrm{max,Pb}j}\theta_{\mathrm{Pb},j} \tag{10}$$

where $Q_{\mathrm{max},j}$ stands for the maximum number of moles of sites (in mol kg^{-1}) available for the protonation of each modal distribution (*j*), while $Q_{\mathrm{max,Pb},j}$ refers to the maximum Pb loading to the modal distribution *j* (Rey-Castro et al., 2009).

3.2 Conditional Affinity Spectra

Gaining physical insight into the isotherm description of the Pb binding is possible via the affinity spectrum formalism, consisting of a distribution function that indicates for each affinity value, the density of an equivalent set of langmuirian independent sites yielding the same total coverage for each metal concentration. Bicomponent isotherms

(e.g. describing the binding of Pb and H) might have associated two-dimensional affinity spectra. However, by fixing the concentration of one component (e.g. fixing pH), the isotherm becomes monocomponent and a one-dimensional affinity spectrum can be analytically derived (Sips, 1948). The obtained density function $\mathrm{p}\left(\log k'_{\mathrm{Pb}}; c_{\mathrm{H}} = \mathrm{cnt}\right)$ is called the Conditional Affinity Spectrum (CAS) (Garcés et al., 2006) because it reflects a specific restriction (such as a fixed pH). The CAS indicates the density of sites with effective affinity $\log k'_{\mathrm{Pb}}$ at a given pH. The effective affinity corresponds to the intrinsic affinity of the site once the energy expended in extracting the protons is considered. From the CAS, the coverage can be computed with

$$\theta_{\mathrm{Pb}}\left(c_{\mathrm{H}} = \mathrm{cnt}, c_{\mathrm{Pb}}\right) = \int_{-\infty}^{\infty} \mathrm{p}\left(\log k'_{\mathrm{Pb}}; c_{\mathrm{H}} = \mathrm{cnt}\right) \frac{k'_{\mathrm{Pb}} c_{\mathrm{Pb}}}{1 + k'_{\mathrm{Pb}} c_{\mathrm{Pb}}} d \log k'_{\mathrm{Pb}} \qquad (11)$$

Due to the linear nature of integration, when the coverage can be expressed as a linear combination of a NICA isotherm for each modal distribution (e.g. a carboxylic, a phenolic and a nitrogen term), the CAS of the whole isotherm will be expressed as the same combination of the CAS of each modal distribution.

$$\mathrm{p}_{\mathrm{fraction}}\left(\log k'_{\mathrm{Pb}}; c_{\mathrm{H}} = \mathrm{cnt}\right) = \frac{\sum_{j=1}^{2\,or\,3} Q_{\mathrm{max,Pb},j}\ \mathrm{p}_j\left(\log k'_{\mathrm{Pb}}; c_{\mathrm{H}} = \mathrm{cnt}\right)}{\sum_{j=1}^{2\,or\,3} Q_{\mathrm{max,Pb},j}} \qquad (12)$$

The application of Sips inversion expression to the NICA isotherm given in eqn. (9) yields the density distribution of a specific modal distribution *j* as (Puy et al., 2008;Puy et al., 2009)

$$\mathrm{p}_j\left(\log k'_{\mathrm{Pb}};c_{\mathrm{H}}=\mathrm{cnt}\right)=\frac{\ln(10)}{\pi}\frac{\left(\bar{k}_{\mathrm{Pb},j}/k'_{\mathrm{Pb}}\right)^{n_{\mathrm{Pb},j}}M_j^{p_j-1}}{1+M_j^{2p_j}+2M_j^{p_j}\cos\left(p_j\phi_j\right)}\left[\sin\left(\pi n_{\mathrm{Pb},j}-\left(1-p_j\right)\phi_j\right)+M_j^{p_j}\sin\left(\pi n_{\mathrm{Pb},j}-\phi_j\right)\right] \quad (13)$$

where

$$M_j\left(c_{\mathrm{H}},k'_{\mathrm{Pb}}\right)=\left[\left(\bar{k}_{\mathrm{H},j}c_{\mathrm{H}}\right)^{2n_{\mathrm{H},j}}+\left(\bar{k}_{\mathrm{Pb},j}/k'_{\mathrm{Pb}}\right)^{2n_{\mathrm{Pb},j}}+2\left(\bar{k}_{\mathrm{H},j}c_{\mathrm{H}}\right)^{n_{\mathrm{H},j}}\left(\bar{k}_{\mathrm{Pb},j}/k'_{\mathrm{Pb}}\right)^{n_{\mathrm{Pb},j}}\cos\left(\pi n_{\mathrm{Pb},j}\right)\right]^{1/2} \quad (14)$$

and

$$\cos\left(\phi_j\right)=\frac{\left(\bar{k}_{\mathrm{H},j}c_{\mathrm{H}}\right)^{n_{\mathrm{H},j}}+\left(\bar{k}_{\mathrm{Pb},j}/k'_{\mathrm{Pb}}\right)^{n_{\mathrm{Pb},j}}\cos\left(\pi n_{\mathrm{Pb},j}\right)}{M_j} \quad (15)$$

Due to linearity, the CAS of different fractions *i* (extracted from the same water) can be weighted by the relative amount of each fraction to yield a global CAS of the whole DOM present at a sampling site:

$$\mathrm{p}_{\mathrm{DOM}}=\frac{\sum_{i=1}^{number\ of\ fractions}w_i\,\mathrm{p}_{\mathrm{fraction},i}}{\sum_{i=1}^{number\ of\ fractions}w_i} \quad (16)$$

4. RESULTS AND DISCUSSION

4.1 Organic Materials

The measurement of DOC during the fractionation allows knowing the representative percentage of each fraction (100% representing the DOC in the original water). Upstream from Paris, the hydrophobic fraction represents more than 60% of DOC (Pernet-Coudrier et al., 2010). Due to WWTP discharges, which contain more than 40% of DOC in the form of hydrophilic fraction and less than 40% of DOC in the form of

hydrophobic fraction, a strong enrichment in the hydrophilic fraction was observed downstream of Paris at Andresy whereas the transphilic fraction is always around ~15-20% of DOC. For the A1 fractions, which correspond to the Achères sampling site, as the hydrophilic character of the sample increases (HPO < TPI < HPI), the percentage of C decreases, while that of N increases (see Table). Also, the degree of unsaturation (e.g. due to rings or multiple bonds) decreases and the average oxidation number of C increases. As already shown (Pernet-Coudrier et al., 2010), the hydrophilic nature of EfOM (Effluent Organic Matter, site A1) stems from the high content of polar functional groups, especially N-containing groups (amides and amines), which is consistent with the observation of abundant proteinaceous structures by Py-GC-MS, fluorescence and FTIR.

4.2 Proton Binding by DOM Fractions

Fig. shows a very small influence of the ionic strength (at 0.1 and 0.05 mol L^{-1}) on the proton binding curve for two different HPO fractions, similarly, for example, to H titrations in (Christl and Kretzschmar, 2001). As a change of the ionic strength modifies the electrostatic component of the binding energy, the mild ionic strength influence indicates a limited impact of the electrostatic component on the binding and prevents a quantitative description of this effect with these data. Thus, no electrostatic correction will be considered in this work, and, although it seems not to be relevant in our fractions, the recovered parameters can be considered conditional to the ionic strength 0.1 mol L^{-1} used in the present work. Croue and co-workers (Croue et al., 2003) have also shown that nonspecific binding starts to be really significant in terms of percentage

of metal bound at high metal loadings (>10^{-5} mol L^{-1}), which are mostly not environmentally relevant.

In the proton titrations (see Fig.), the fraction HPIA1 reveals a pattern close to a triple wave, while the other fractions exhibit the typical double wave behaviour: HPOA1 and TPIA1 fractions lie very close to one another, and HPOAN and HPOMT also remain very close, but showing a higher Q_{max} than HPOA1 and TPIA1. This behaviour suggests applying a bimodal distribution for modelling these four proton distributions of sites, though for the HPIA1 fraction a trimodal distribution is more suitable. Previously, (Plette et al., 1995) and (Croue et al., 2003) also used a trimodal distribution to describe the behaviour of nitrogen-enriched organic materials. For the sake of simplicity, in bimodal distributions, the modal distribution 1 is labelled "carboxylic" and the modal distribution 2 is labelled "phenolic", although the reality is much more complex. In the trimodal fraction HPIA1, the carboxylic and phenolic groups could correspond to the first and the third modal distribution, respectively, in agreement with the pH range where they develop. Therefore, the second modal distribution in HPIA1 might be (just for a simple labelling) designed as N-containing groups. Nevertheless, the third distribution called "phenolic" could also contain Nitrogen atoms, since the HPI fraction displays a very low content of aromatic rings (Pernet-Coudrier et al 2010) and, therefore, cannot have such an amount of phenolic groups.

The computation of the HPIA1 protonation curve with eqn. (8) requires the concentration of neutral sites (see eqn. (6)). We estimated $Q'_{max,Neutral}$ by assuming that 40% of the nitrogen content is yielding such type of sites, given that this estimation leads to a near-zero charge for HPIA1 (quite close to the one of the TPIA1 fraction) at pH 3. At this low pH, the amino sites (specific of this fraction) are expected to be protonated (Croue et al., 2003).

Fitted NICA parameters describing the proton binding to the respective fractions and modal distributions are gathered in Table 3. The fitted values are in agreement with the observations commented above. HPIA1 shows the highest total charge (Q_{max1}+ Q_{max2}+ Q_{max3}= 10.55 mol kg^{-1}), while HPOAN or HPOMT show a similar value, roughly one half of that of HPIA1. The proton titrations depicted in Fig. confirmed the high content of functional groups in HPIA1 and corroborate previous observations (Pernet-Coudrier et al., 2010). The other two fractions, HPOA1 and TPIA1, show the lowest total charge, with very little difference between them.

As expected, pH values corresponding to the fitted $\log \overline{k}_{H,i}$ values correspond to the rising ranges of each wave in Fig. , while m_i values are related to the width of the corresponding modal affinity spectrum, hence, a lower m_i value indicates a greater heterogeneity in the distribution and a lower slope of the titration curve. Actually, a smaller slope (i.e. a more elongated titration curve) reflects that the proton binding takes place in a wider pH range and corresponds to a wider range of proton binding affinities. Notice that the charge of the fractions HPOAN and HPOMT is not zero at pH 3, meaning that strong acid sites seem to be present within these fractions. Accordingly, the range of pH to which the first modal distribution of these fractions spans is wider than the range covered by the titration curve depicted in Fig. 3, thus justifying the lower m_1 value reached (0.50 and 0.45) in comparison with the m_1 in both HPOA1 and TPIA1 fractions (0.66 and 0.74). Moreover, $Q_{max,2}$ is smaller than $Q_{max,1}$ for all the fractions except HPIA1, with the modal distributions of this fraction being (Table 3) more homogeneous than most of the distributions of the other fractions.

A full comparison of the $\log \overline{k}_{H,i}$ with published data (with the generic NICA-Donnan values for humic and fulvic acids (Milne et al., 2001) or with hydrophilic and transphilic fractions (Milne et al., 2003)) has to take into account that in the present

study, at 0.1 M ionic strength, the electrostatic contribution has not been subtracted. Thus, the $\log \bar{k}_{\mathrm{H},i}$ obtained are consistent with the ones published in these previous works, as they tend to show slightly higher values due to the inclusion of electrostatics. Even though the binding behaviour of humic fractions can be described with generic binding parameters (Milne et al., 2001;Ritchie and Perdue, 2003), the high maximum charge of the most hydrophilic fraction as well as the proton binding differences between the hydrophilic and hydrophobic DOM, as shown above, suggest that a comprehensive knowledge of DOM composition is required in order to avoid errors in metal speciation and risk assessment. This finding was recently demonstrated for forest soil (van Schaik et al., 2010).

4.3 Pb Binding by DOM Fractions

4.3.1 Pb Binding Described with NICA Isotherm

Taking into account the recommendation of producing environmentally relevant data (Town and Filella, 2002), 20 mg L^{-1} of each organic fraction was used for the experiments. The experimental results of Pb binding to the DOM fractions discussed above are depicted in Fig. at different pH. The titrations of HPOA1 and TPIA1 at pH 4.5 were discarded due to the poor data quality. In contrast, as a result of the very strong complexation of Pb to HPIA1 at alkaline pH values (pH 9), the free Pb concentration lies below the AGNES detection limit under the conditions specified in the present work. When increasing the Pb concentration, both coagulation and precipitation of DOM occur.

436 The corresponding fitted parameters that describe the Pb binding with the NICA
437 isotherm are listed in Table 4. Within a fraction, a clear positive correlation exists
438 between log $k_{H,j}$ and log $k_{Pb,j}$ of the different modal distributions. However, for a given
439 modal distribution, the order of the fractions according to log $k_{H,j}$ differs quite
440 substantially from the order according to log $k_{Pb,j}$ indicating important differences
441 between the carboxylic (or phenolic) distributions from one fraction to the next. The
442 conditional log $k_{Pb,j}$ values obtained here for the different fractions are slightly higher
443 and consistent with the generic values obtained for humic and fulvic acids (Milne et al.,
444 2003) with the NICA-Donnan model.

445 As regards maximum capacity, generally, $Q_{max,Pb,i} < Q_{max,i}$, the differences between the
446 maximum capacity of H, $Q_{max,i}$, and that of Pb, $Q_{max,Pb,i} = \frac{n_{Pb,i}}{n_{H,i}} Q_{max,i}$, in each modal
447 distribution being due to the $\frac{n_{Pb,i}}{n_{H,i}}$ factors (Kinniburgh et al., 1999;Koopal et al.,
448 2001;Koopal et al., 2005). For instance, $Q_{max,Pb,3}$ of HPIA1 (3.66 mol kg^{-1}) equals 60%
449 of $Q_{max,3}$ (6.12 mol kg^{-1}). Like in the proton binding, HPIA1 displays the maximum Pb
450 binding capacity (i.e the sum $Q_{max,Pb,1}$+ $Q_{max,Pb,2}$+ $Q_{max,Pb,3}$ = 6.32 mol kg^{-1}) among all
451 the fractions analysed in this work.

452 *4.3.2 Pb Binding Visualised with CAS*
453

454 The Conditional Affinity Spectra will now help to compare the various binding
455 properties of the different DOM fractions. The corresponding CAS are shown in Fig. 5.
456 The full CAS of the fraction is represented in the left column of figures (panel "a"),
457 while figures in the right column (panel "b") depict each modal distribution within the
458 DOM fractions. It should be noted that in all plots, the area of the CAS of the whole
459 fraction (one curve in the left column) integrates to 1, consequently, the plots shown in

Fig. 5 do not reflect the relative abundance of the various fractions in water, while the relative area of the different modal distributions in the right column does reflect the proportion of each modal distribution in this fraction. Therefore, the area of each modal distribution in the right plots is proportional to its maximum capacity, and the direct addition of these curves leads to the corresponding plot on the left.

Fig. 5.1.a depicts the CAS of the HPOA1 fraction and the change of this distribution with pH (pH 4-9). As pH decreases, the distribution shifts towards lower affinities, this shift reflecting the increasing energy expended in extracting the protons required for the Pb binding. Fig. 5.1.b shows that this shift is mainly due to the phenolic distribution (distribution 2) indicating that protonation in the 9-to-5 pH range takes place mainly in the phenolic distribution (distributions 1 at pH 7 and 9 are superimposed). Remark that even though Pb will, at pH 9, bind preferably to the "phenolic" sites, at pH 5 both distributions overlap to a greater extend. The Pb binding (for low loadings) to the carboxylic distribution will then be dominant (see Table 5), due to the higher abundance of the carboxylic sites at higher affinities (Puy et al., 2008;Rey-Castro et al., 2009). Accordingly, Fig. 5.1.a evolves from a double peaked shape at pH 9 to a single peak at pH below 7. A similar behaviour is apparent in the phenolic distribution of the TPIA1 fraction (see Figs. 5.2.a and 5.2.b).

With respect to HPOAN and HPOMT fractions (see Figs. .3 and .4), the phenolic distribution determines the binding (for low Pb concentrations) at pH 9 in both fractions, but at pH 5 the binding in both cases is dominated by the carboxylic distribution due to the low complexation (smaller area) of the phenolic groups (see Figs. .3.b and Figs. .4.b). Notice the deformation of the carboxylic distribution from pH 7 to pH 5 in the case of HPOAN. The deformation of the carboxylic distribution implies that the strongest proton binding sites, which become protonated from pH 7 to 5, are also the

485 strongest Pb sites, i.e. the change in CAS is indicating a strong correlation between the
486 binding energies of H and Pb in the carboxylic distribution (Puy et al., 2009;Puy et al.,
487 2008;Rey-Castro et al., 2009).
488 Figs. 5.5.a and b plot the CAS for the HPIA1 fraction. The highest affinity sites (mode
489 3), with the strongest binding affinity for Pb at pH 9, show the weakest affinity at pH 5.
490 Such a large shift experienced by mode 3 from pH 9 to 5 is mainly due to the strong
491 binding affinity that this distribution presents for the proton, hence, the energy
492 expended to extract protons increases when pH decreases. Since mode 3 also contains
493 the highest maximum Pb capacity, its environmental impact will be highly pH
494 dependent.
495

496 4.4 Global Pb binding behaviour

497 A global CAS for Pb binding to the DOM of sampling site A1 can be obtained from the
498 weighted addition of the CAS of the different fractions according to the DOM mass
499 proportion of each fraction in the water: HPOA1: 31%; TPIA1: 20% and HPIA1: 49%.
500 It should be pointed out that the shape in the resulting affinity distribution changes
501 when pH changes (pH 5-9) (Fig.). The figure also depicts the occupied sites for a given
502 free Pb concentration of 10 μg L^{-1}. In this case, from pH 5 to 9, 50-60% of the bound Pb
503 is adsorbed at the HPIA1 fraction, while the HPOA1 and the TPIA1 fractions contain
504 respectively around 20-30% and 14-18% of the bound Pb (see Table). If the free Pb
505 concentration is reduced to 0.1 μg L^{-1}, the roles of the different fractions are similar,
506 with a small increase of the percentage bound to the TPIA1 fraction. However, the
507 distribution inside all the fractions remains in all cases highly pH dependent as indicated
508 in Table b. This result could be expected looking at the pH effect on the modal
509 distributions described in the preceding section. Nevertheless, at environmental pH (7-8

in the Seine Basin) and regardless of the Pb loadings, around 50% of Pb bound to HPIA1 is attached to the second modal distribution, e. g. complexed by the nitrogen sites. This feature means that the second affinity sites, which are labelled as nitrogen groups, are important binding sites in urban aquatic systems, since they complex 0.49×0.48=24% of the bound Pb. This feature was also shown with Cu (Croue et al., 2003).

Given that hydrophobic fractions, such as humics and fulvics, are always the most important fractions of DOM in the literature (Town and Filella, 2002), we performed a computation with a mixture of 50 % of HPOAN (humics and fulvics from Seine River at Andrésy) and 50 % of HPIA1 (main fraction from WWTP effluent). Such a mixture does not physically exist due, at least, to the presence of the others fractions. Nevertheless, the results presented in Table show, that regardless of the Pb loadings, at environmental pH (7-8), between 82 and 90 % of Pb is bound to the HPI fraction, thus, overcoming by a wide margin the complexation to humics and fulvics (HPO) from the river. Even though this computation is not fully representative of the real media and merely extrapolates the experimental data, it still demonstrates, for the first time, that the hydrophilic fraction can exert a greater impact in Pb binding than humic substances. This feature also highlights that Pb speciation in surface water under high human pressure should include, not only the humic and/or fulvic part of DOC, but also other more hydrophilic fractions.

4.5 Broader environmental implications

The high binding capacity of HPIA1, which is also the predominant EfOM fraction discharged by the WWTP in the river Seine (inducing a twofold increase of DOC),

535 could strongly influence the fate and transport of lead in the aquatic system. Generally,
536 speciation of dissolved lead is controlled by dissolved organic matter. Dissolved organic
537 complexes of lead in water bodies could represent more than 90% of total dissolved
538 lead according to the nature of dissolved organic matter (Linnik, 2003). In a recent
539 study, spatio-temporal changes in the concentrations of dissolved Pb in an urban stream
540 were strongly related to quantity and quality of DOM (Park, 2009).
541 In addition to controlling dissolved lead speciation, dissolved organic matter could also
542 be responsible for the release of Pb and other metals from the sediment to the water
543 column, as it has been already observed downstream of Paris (Garban et al., 1996).
544 Moreover, another study suggests a possible removal of trace metals from suspended
545 particulate matter by dissolved organic matter resulting in an increase of dissolved trace
546 metal concentration (Shafer et al., 1997). Given that Pb in association with large
547 particles is likely to be more rapidly removed by sedimentation from the water column
548 than that associated with DOM, Pb transport could be increased due to the high binding
549 capacity of EfOM. Furthermore, the hydrophilic fraction, due to its small molecular
550 weight and weak aromaticity compared to humic (Pernet-Coudrier et al., 2010) may
551 have low affinity to particles (Specht et al., 2000;Vermeer et al., 1998). Besides, (Nam
552 et al., 2008) have recently shown that effluent organic matter exhibits, in average, a
553 lower biodegradability compared to natural organic matter, except the polysaccharides
554 compounds that were removed during a 21-day test, but were not detected in our HPI
555 fraction (Pernet-Coudrier et al., 2010). Then, the combination of all these characteristics
556 (high affinity and binding capacity to Pb, low affinity for particles, low
557 biodegradability) indicates that hydrophilic organic matter from WWTP plays an
558 important role in the biogeochemical cycle of Pb, since it may greatly enhance its
559 transport.

Furthermore, the strong complexation of Pb to the HPI fraction will decrease the free Pb concentration and, thus, for conditions where FIAM (Free Ion Activity Model) applies, the availability of Pb will be lower than expected with humics. Lead bioavailability depends not only on the free lead concentration, but also on the nature of complexing ligands. For instance, some authors have shown that Pb uptake in the presence of humic substances was higher than predicted from measured free metal concentrations due to formation of ternary complexes between lead, humic substances and internalization sites of cell walls (Lamelas et al., 2009;Lamelas et al., 2005;Lamelas and Slaveykova, 2007). Therefore, due to its specific characteristics the hydrophilic ligands may better protect aquatic life from lead toxicity compared to humic susbtances. It seems, then, timely the study of the influence of the hydrophilic fraction of dissolved organic matter on lead bioavailability in rivers under high urban pressure.

Conclusions

Different organic fractions extracted from the Seine river and from WWTP effluents have been separated according to their hydrophilic character and purified. All the isolated fractions were studied in regards of their proton and lead binding capacities. For the first time, Pb binding parameters of the hydrophilic fraction of an urbanized aquatic system were obtained by using the new technique AGNES.

The influence of the ionic strength on the acid-base behaviour was nearly negligible. The proton binding characteristics justify the use of bimodal distributions for the

586 binding sites of all the organic fractions, except for the most hydrophilic one, which
587 requires a trimodal distribution.
588 Both, the maximum number of protonable groups and the maximum binding capacity of
589 Pb attain their maximum value (per gram of fraction) at the most hydrophilic fraction
590 (HPIA1). The NICA description of the Pb binding results implies major differences
591 between the maximum complexation capacities of H and those of Pb for the different
592 modal distributions within each organic fraction.
593 The characteristics of these various fractions with respect to Pb binding have been
594 visualized by plotting the CAS associated with each fraction. The CAS indicates the
595 effective distribution of affinities shown by the organic fraction. pH largely modifies the
596 strongest affinity distribution, so that at alkaline pH (pH=9) Pb binding is determined by
597 the "phenolic" distribution, whereas at acidic pH (pH=5) both distributions compete to a
598 greater extent, with the "carboxylic" distribution being responsible for binding to the
599 HPO fractions.
600 The CAS of the different fractions can also be combined into a global CAS of all the
601 DOM present at a sampling site, thus allowing a unified visual characterization of the
602 binding properties of the water. At environmental levels of both free Pb and pH, the HPI
603 fraction from WWTP effluents is the fraction with the highest percentage of bound Pb.
604 This feature highlights that, at least in surface water under high human pressure, the
605 study of Pb speciation should not be restricted to just the humic and/or fulvic part of
606 DOC .
607 Furthermore, the modification of lead speciation in rivers under high urban pressure due
608 to the hydrophilic fraction of the effluent organic matter could have implications in the
609 lead bioavailability. Future work is needed to determine the extent and the conditions
610 under which EfOM and especially HPI fraction plays an important role in the transport

and interaction with particles and in attenuating metal uptake by aquatic organisms as a result of both the decrease of free lead concentration and/or the lability characteristics of the corresponding lead complexes.

Acknowledgements

This work has been financially supported by the French Ministry of Research and Education (Ph.D. grant), the French National Research Agency (ANR, project BIOMET JC05_59809) and by the Spanish Ministry of Education and Science (Projects CTQ2006-14385, CTM2006-13583, CTQ2009-07831 and CTQ2009-14612) and by the "Comissionat per a Universitats i Recerca del Departament d'Innovació, Universitats i Empresa de la Generalitat de Catalunya".

References

1. Buffle J. (1988) *Complexation Reactions in Aquatic Systems. An Analytical Approach.* Ellis Horwood Limited, Chichester. UK.

2. Buzier R., Tusseau-Vuillemin M. H., Meriadec C. M. D., Rousselot O., and Mouchel J. M. (2006) Trace metal speciation and fluxes within a major French wastewater treatment plant: Impact of the successive treatments stages. *Chemosphere* **65**, 2419-2426.

3. Chakraborty P. and Chakrabarti C. L. (2008) Competition from Cu(II), Zn(II) and Cd(II) in Pb(II) binding to Suwannee River Fulvic Acid. *Water Air Soil Poll.* **195**, 63-71.

4. Christl I. and Kretzschmar R. (2001) Relating ion binding by fulvic and humic acids to chemical composition and molecular size. 1. Proton binding. *Environ. Sci. Technol.* **35**, 2505-2511.

5. Christl I., Metzger A., Heidmann I., and Kretzschmar R. (2005) Effect of humic and fulvic acid concentrations and ionic strength on copper and lead binding. *Environ. Sci. Technol.* **39**, 5319-5326.

6. Companys E., Cecília J., Codina G., Puy J., and Galceran J. (2005) Determination of the concentration of free Zn^{2+} with AGNES using different strategies to reduce the deposition time. *J. Electroanal. Chem.* **576**, 21-32.

7. Companys E., Garcés J. L., Salvador J., Galceran J., Puy J., and Mas F. (2007a) Electrostatic and specific binding to macromolecular ligands. A general analytical expression for the Donnan volume. *Colloids Surf. A* **306**, 2-13.

8. Companys E., Puy J., and Galceran J. (2007b) Humic acid complexation to Zn and Cd determined with the new electroanalytical technique AGNES. *Environ. Chem.* **4**, 347-354.

9. Croue J. P. (2004) Isolation Of Humic And Non-Humic Nom Fractions: Structural Characterization. *Environmental Monitoring and Assessment* **92**, 193-207.

10. Croue J. P., Benedetti M. F., Violleau D., and Leenheer J. A. (2003) Characterization and copper binding of humic and nonhumic organic matter isolated from the South Platte River: Evidence for the presence of nitrogenous binding site. *Environ. Sci. Technol.* **37**, 328-336.

11. Domingos R.F., Huidobro C., Companys E., Galceran J., Puy J., and Pinheiro J. P. (2008) Comparison of AGNES (Absence of Gradients and Nernstian Equlibrium Stripping) and SSCP (Scanned Stripping Chronopotenciometry) for Trace Metal Speciation Analysis. *J. Electroanal. Chem.* **617**, 141-148.

12. Filella M., Quentel F., Pernet-Coudrier B., and Varrault G. (2009) Application of a refractory organic matter quantification method to wastewater effluents. *INT. J. ENVIRON. ANAL. CHEM.* **89**, 799-807.

13. Filella M. and Town R. M. (2000) Determination of metal ion binding parameters for humic substances Part 1. Application of a simple calculation method for extraction of meaningful parameters from reverse pulse polarograms. *J. Electroanal. Chem.* **485**, 21-33.

14. Galceran J., Companys E., Puy J., Cecília J., and Garcés J. L. (2004) AGNES: a new electroanalytical technique for measuring free metal ion concentration. *J. Electroanal. Chem.* **566**, 95-109.

15. Galceran J., Huidobro C., Companys E., and Alberti G. (2007) AGNES: a technique for determining the concentration of free metal ions. The case of Zn(II) in coastal Mediterranean seawater. *Talanta* **71**, 1795-1803.

16. Garban B., Ollivon D., Carru A. M., and Chesterikoff A. (1996) Origin, retention and release of trace metals from sediments of the River Seine. *Water Air Soil Poll.* **87**, 363-381.

17. Garcés J. L., Mas F., and Puy J. (2006) Conditional equilibrium constants in multicomponent heterogeneous adsorption: The conditional affinity spectrum. *J. Chem. Phys.* **124**, 044710-1-14.

18. Gustafsson J. P. (2000) Visual MINTEQA2. Sofware. http://www.lwr.kth.se/english/OurSoftware/vminteq/index.htm

19. Imai A., Fukushima T., Matsushige K., Kim Y. H., and Choi K. (2002) Characterization of dissolved organic matter in effluents from wastewater treatment plants. *Water. Res.* **36**, 859-870.

20. Kinniburgh D. G., van Riemsdijk W. H., Koopal L. K., Borkovec M., Benedetti M. F., and Avena M. J. (1999) Ion binding to natural organic matter: competition, heterogeneity, stoichiometry and thermodynamic consistency. *Colloids Surf. A* **151**, 147-166.

21. Koopal L. K., Saito T., Pinheiro J. P., and van Riemsdijk W. H. (2005) Ion binding to natural organic matter: General considerations and the NICA-Donnan model. *Colloids Surf. A* **265**, 40-54.

22. Koopal L. K., van Riemsdijk W. H., Dewit J. C. M., and Benedetti M. F. (1994) Analytical isotherm equations for multicomponent adsorption to heterogeneous surfaces. *J. Colloid. Interf. Sci.* **166**, 51-60.

23. Koopal L. K., van Riemsdijk W. H., and Kinniburgh D. G. (2001) Humic matter and contaminants. General aspects and modeling metal ion binding. *Pure Appl. Chem.* **73**, 2005-2016.

24. Lamelas C., Pinheiro J. P., and Slaveykova V. I. (2009) Effect of Humic Acid on Cd(II), Cu(II), and Pb(II) Uptake by Freshwater Algae: Kinetic and Cell Wall Speciation Considerations. *Environ. Sci. Technol.* **43**, 730-735.

25. Lamelas C. and Slaveykova V. I. (2007) Comparison of Cd(II), Cu(II), and Pb(II) biouptake by green algae in the presence of humic acid. *Environ. Sci. Technol.* **41**, 4172-4178.

26. Lamelas C., Wilkinson K. J., and Slaveykova V. I. (2005) Influence of the composition of natural organic matter on Pb bioavailability to microalgae. *Environ. Sci. Technol.* **39**, 6109-6116.

27. Leenheer J. A. et al. (2000) Comprehensive isolation of natural organic matter from water for spectral characterizations and reactivity testing. American Chemical Society, Washington DC, pp. 68-83.

28. Linnik P. N. (2003) Complexation as the most important factor in the fate and transport of heavy metals in the Dnieper water bodies. *Anal. Bioanal. Chem.* **376**, 405-412.

29. Milne C. J., Kinniburgh D. G., and Tipping E. (2001) Generic NICA-Donnan model parameters for proton binding by humic substances. *Environ. Sci. Technol.* **35**, 2049-2059.

30. Milne C. J., Kinniburgh D. G., van Riemsdijk W. H., and Tipping E. (2003) Generic NICA-Donnan model parameters for metal-ion binding by humic substances. *Environ. Sci. Technol.* **37**, 958-971.

31. Nam S. N., Krasner S. W., and Amy G. L. (2008) Differentiating effluent organic matter (EfOM) from natural organic matter (NOM): Impact of EfOM on drinking water sources. *Advanced Environmental Monitoring* 259-270.

32. Nriagu J. O. (1996) History of Global Metal Pollution. *Science* **272**, 223-224.

33. Park J. H. (2009) Spectroscopic characterization of dissolved organic matter and its interactions with metals in surface waters using size exclusion chromatography. *Chemosphere* **77**, 485-494.

34. Pernet-Coudrier B. (2008) Influence de la matière organique dissoute sur la speciation et la biodisponibilité des metaux: cas de la Seine, un milieu sous forte pression urbaine. Université Paris-Est.

35. Pernet-Coudrier B., Clouzot L., Varrault G., Tusseau-Vuillemin M. H., Verger A., and Mouchel J. M. (2008) Dissolved organic matter from treated effluent of a major wastewater treatment plant: Characterization and influence on copper toxicity. *Chemosphere* **73**, 593-599.

36. Pernet-Coudrier B. et al. (2010) Characterization of dissolved organic matter in Parisian urban aquatic systems: predominance of hydrophilic and proteinaceous structures.

37. Pinheiro J. P., Mota A. M., and Benedetti M. F. (1999) Lead and calcium binding to fulvic acids: Salt effect and competition. *Environ. Sci. Technol.* **33**, 3398-3404.

38. Plette A. C. C., Vanriemsdijk W. H., Benedetti M. F., and Vanderwal A. (1995) Ph Dependent Charging Behavior of Isolated Cell-Walls of A Gram-Positive Soil Bacterium. *J. Colloid. Interf. Sci.* **173**, 354-363.

39. Puy J., Galceran J., Huidobro C., Companys E., Samper N., Garcés J. L., and Mas F. (2008) Conditional Affinity Spectra of Pb^{2+}-Humic Acid Complexation from Data Obtained with AGNES. *Environ. Sci. Technol.* **42**, 9289-9295.

40. Puy J., Huidobro C., David C., Rey-Castro C., Salvador J., Companys E., Garces J. L., Galceran J., Cecilia J., and Mas F. (2009) Conditional affinity spectra underlying NICA isotherm. *Colloids Surf. A* **347**, 156-166.

41. Rey-Castro C., Mongin S., Huidobro C., David C., Salvador J., Garces J. L., Galceran J., Mas F., and Puy J. (2009) Effective Affinity Distribution for the Binding of Metal Ions to a Generic Fulvic Acid in Natural Waters. *Environ. Sci. Technol.* **43**, 7184-7191.

42. Ritchie J. D. and Perdue E. M. (2003) Proton-binding study of standard and reference fulvic acids, humic acids, and natural organic matter. *Geochim. Cosmochim. Ac.* **67**, 85-96.

755 43. Sarathy V. and Allen H. E. (2005) Copper complexation by dissolved organic
756 matter from surface water and wastewater effluent. *Ecotox. Environ. Safe.* **61**,
757 337-344.

758 44. Shafer M. M., Overdier J. T., Hurley J. P., Armstrong D., and Webb D. (1997)
759 The influence of dissolved organic carbon, suspended particulates, and hydrology
760 on the concentration, partitioning and variability of trace metals in two contrasting
761 Wisconsin watersheds (USA). *Chemical Geology* **136**, 71-97.

762 45. Sips R. (1948) On the structure of a catalyst surface. *J. Chem. Phys.* **16**, 490-495.

763 46. Specht C. H., Kumke M. U., and Frimmel F. H. (2000) Characterization of NOM
764 adsorption to clay minerals by size exclusion chromatography. *Water. Res.* **34**,
765 4063-4069.

766 47. Tessier A. and Turner D. R. (1995) *Metal Speciation and Bioavailability in*
767 *Aquatic Systems*. John Wiley & Sons, Chichester. UK.

768 48. Thurman E. M. and Malcolm R. L. (1981) Preparative Isolation of Aquatic Humic
769 Substances. *Environ. Sci. Technol.* **15**, 463-466.

770 49. Town R. M. and Filella M. (2002) Implications of natural organic matter binding
771 heterogeneity on understanding lead(II) complexation in aquatic systems. *Sci.*
772 *Total Envir.* **300**, 143-154.

773 50. van Riemsdijk W. H., Bolt G. H., Koopal L. K., and Blaakmeer J. (1986)
774 Electrolyte adsorption on heterogeneous surfaces - Adsorption models. *J. Colloid.*
775 *Interf. Sci.* **109**, 219-228.

776 51. van Schaik J. W. J., Kleja D. B., and Gustafsson J. P. (2010) Acid-base and
777 copper-binding properties of three organic matter fractions isolated from a forest
778 floor soil solution. *Geochim. Cosmochim. Ac.* **74**, 1391-1406.

779 52. Vermeer A. W. P., van Riemsdijk W. H., and Koopal L. K. (1998) Adsorption of
780 humic acid to mineral particles. 1. Specific and electrostatic interactions.
781 *Langmuir* **14**, 2810-2819.

782 53. Zavarise F., Companys E., Galceran J., Alberti G., and Profumo A. (2010)
783 Application of the new electroanalytical technique AGNES for the determination
784 of free Zn concentration in river water. *Anal. Bioanal. Chem.* **397**, 389-394.
785
786
787

Tables

Table 1: Elemental composition of DOM fractions.

Sites	Samples	C (%)	H (%)	O (%)	N (%)	S (%)	Ashes (%)	Sum (%)
Achères (WWTP)	HPOA1	53.6	6.5	27.9	5.7	2.6	2.9	99.2
	TPHA1	48.4	6.4	28.8	8.4	2.1	4.7	98.8
	HPIA1	43.8	7.1	29.4	12.3	2.1	5.0	99.7
Andrésy	HPOAN	50.2	5.1	32.9	3.4	1.9	5.0	98.5
Méricourt	HPOMT	46.5	5.0	31.0	3.1	2.3	4.7	92.6

Table 2: Characteristic parameters of AGNES.

		duration	potential	gain
first stage (aiming at equilibrium)	first substage	$t_{1,a}$	$E_{1,a}$ (diffusion limited conditions for deposition)	$Y_{1,a}$
	second substage	$t_{1,b}$	$E_{1,b}$ (equilibrium potential)	Y (desired gain)
second stage (aiming at quantification)		t_2	E_2 (diffusion limited conditions for re-oxidation)	Y_2

803 Table 3: H binding parameters obtained with NICA fitting. Subscripts 1, 2, and 3 could
804 be (somewhat arbitrarily) labelled as 'carboxylic', "nitrogen" (only for hydrophilic
805 fraction) and 'phenolic'; see section 4.2.

	HPOA1	TPIA1	HPIA1	HPOAN	HPOMT
$\log (\overline{k}_{H,1}$ / mol $L^{-1})$	4.35	4.22	3.51	4.05	3.95
m_1	0.66	0.74	0.60	0.50	0.45
$Q_{max,1}$ / mol kg^{-1}	2.31	2.17	1.70	4.27	4.35
$\log (\overline{k}_{H,2}$ / mol $L^{-1})$	10.09	9.44	6.91	9.28	9.43
m_2	0.30	0.44	0.89	0.65	0.73
$Q_{max,2}$ / mol kg^{-1}	1.57	1.49	2.73	0.61	0.62
$\log (\overline{k}_{H,3}$ / mol $L^{-1})$			9.42		
m_3			0.94		
$Q_{max,3}$ / mol kg^{-1}			6.12		
$Q_{max,H}$ / mol kg^{-1}	3.88	3.66	10.55	4.88	4.97
r^2	1.000	0.999	1.000	1.000	1.000

Table 4: Pb binding parameters obtained with NICA fitting.

	HPOA1	TPIA1	HPIA1	HPOAN	HPOMT
$\log (\overline{k}_{Pb,1}$ / mol $L^{-1})$	2.09	0.21	4.56	2.63	3.10
$n_{Pb,1}$	0.44	0.31	0.67	0.64	0.68
$n_{H,1}$	1.00	1.00	0.97	0.72	0.53
$\log (\overline{k}_{Pb,2}$ / mol $L^{-1})$	7.86	6.80	5.65	8.06	7.83
$n_{Pb,2}$	0.49	0.43	0.51	0.86	0.68
$n_{H,2}$	0.59	0.55	0. 93	1.00	0.73
$\log (\overline{k}_{Pb,3}$ / mol $L^{-1})$			7.19		
$n_{Pb,3}$			0.56		
$n_{H,3}$			0.94		
$Q_{max,Pb,1}$ / mol kg^{-1}	1.01	0.66	1.17	3.80	5.58
$Q_{max,Pb,2}$ / mol kg^{-1}	1.29	1.15	1.49	0.52	0.58
$Q_{max,Pb,3}$ / mol kg^{-1}			3.66		
$Q_{max,Pb}$ / mol kg^{-1}	2.30	1.82	6.32	4.32	6.16
r^2	0.949	0.980	0.937	0.924	0.973

Table 5: Percentages of Pb bound at each fraction (a) and at each modal distribution of each fraction (b) extracted in the sampling site A1 at a given free Pb concentration and pH.

a)

c_{Pb} / μg L^{-1}	pH	HPOA1	TPIA1	HPIA1
10	5	19	14	66
	7	28	16	56
	8	30	18	52
	9	29	16	55
1	5	23	21	55
	7	28	19	53
	8	32	21	47
	9	32	19	49
0.1	5	26	30	43
	7	29	22	49
	8	33	24	43
	9	34	22	44

b)

c_{Pb} / μg L^{-1}	pH	HPOA1		TPIA1		HPIA1		
		1 mode	2 mode	1 mode	2 mode	1 mode	2 mode	3 mode
10	5	74	26	69	31	93	6.9	0.4
	7	47	53	35	65	39	53	8.1
	8	44	56	16	84	20	46	34
	9	10	90	7.4	93	8.1	20	72
1	5	76	24	74	26	91	8.7	0.5
	7	54	46	44	56	44	50	6.4
	8	44	56	22	78	25	47	28
	9	13	87	10	90	9.8	21	69
0.1	5	77	23	78	22	88	11	0.6
	7	59	41	51	49	47	48	5.4
	8	44	56	30	70	29	47	24
	9	17	83	14	86	13	23	65

Table 6: Percentages of Pb bound at each fraction assuming a mixture of 50%HPOAN and 50%HPIA1 at a given free Pb concentration and pH.

c_{Pb} / μg L^{-1}	pH	HPOAN	HPIA1
1	5	11	89
	7	10	90
	8	18	82
	9	28	72
0.1	5	11	89
	7	6.8	93
	8	11	89
	9	19	81

Figures

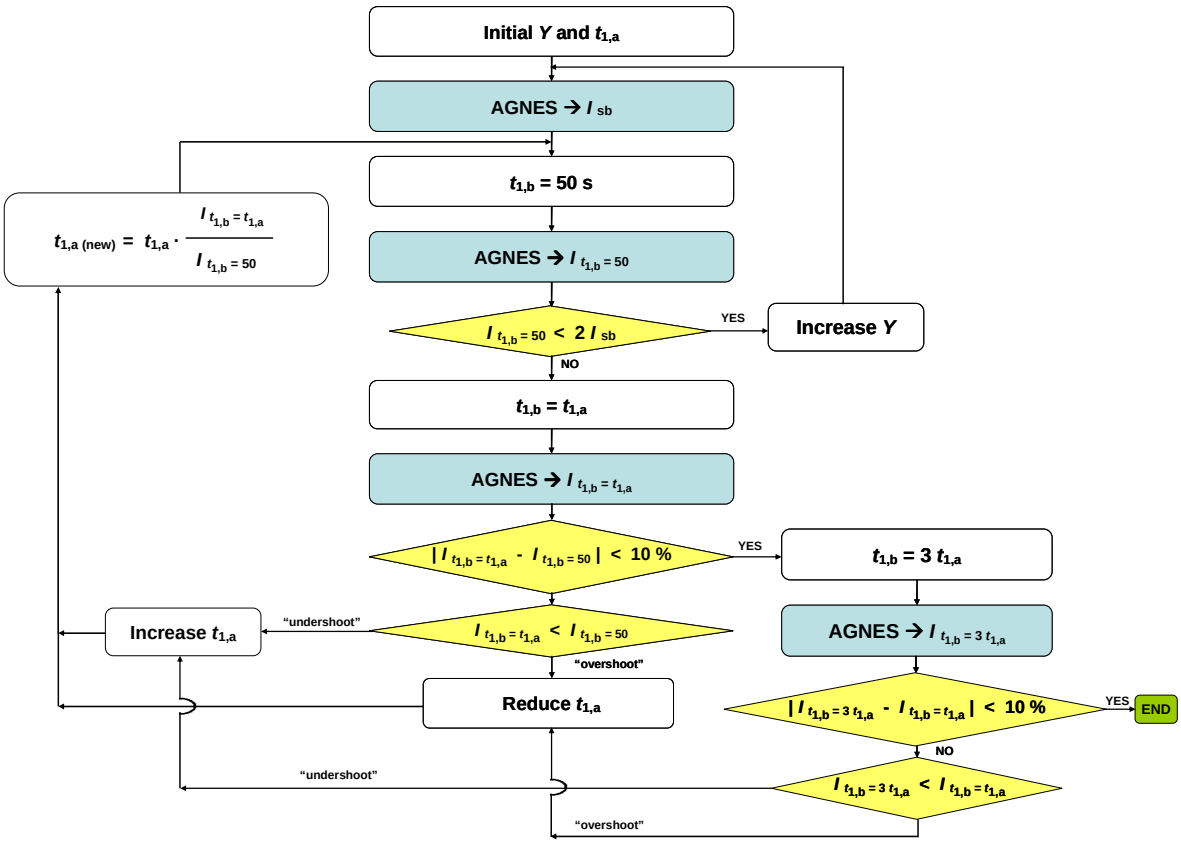

Fig 1: Flow diagram for the selection of parameters in the application of AGNES. For other nomenclature, see table 2 and section 2.3

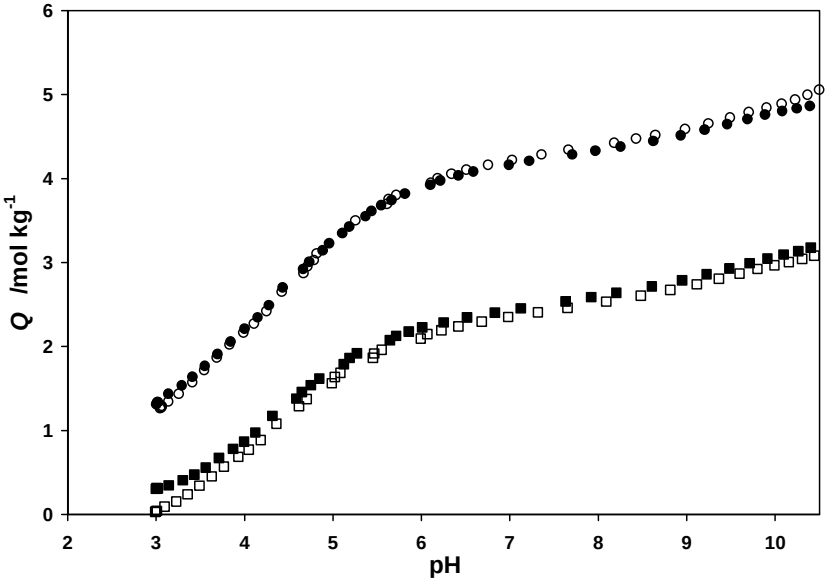

Fig 2: Proton titration of DOM fractions HPOA1 at $I = 0.1$ mol L^{-1} (■) and $I = 0.05$ mol L^{-1} (□) and HPOMT at $I = 0.1$ mol L^{-1} (●) and I = 0.05 mol L^{-1} (○).

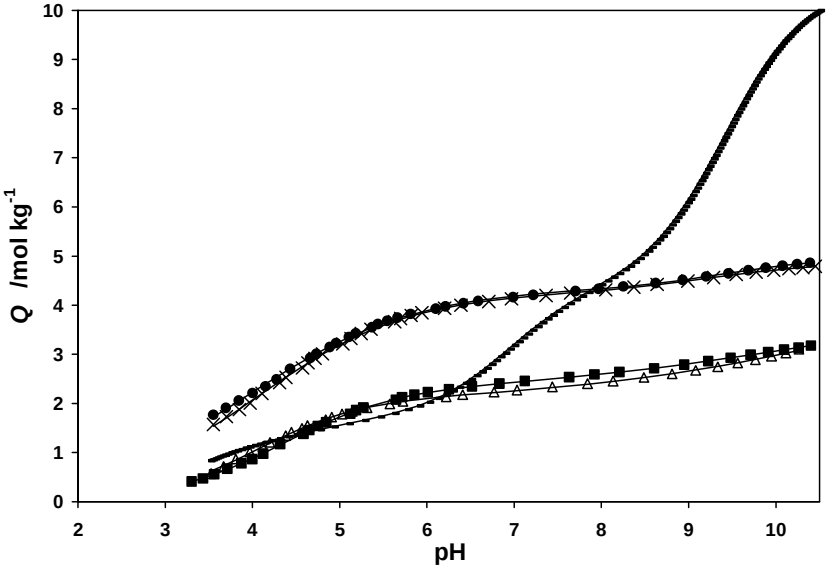

Fig 3: Proton titrations of studied DOM fractions at ionic strength 0.1 mol L^{-1}. HPOA1 (■), TPIA1 (Δ), HPOMT (●), HPOAN (×) and HPIA1 (-). Lines correspond to the fitting of NICA model with parameters in Table 3.

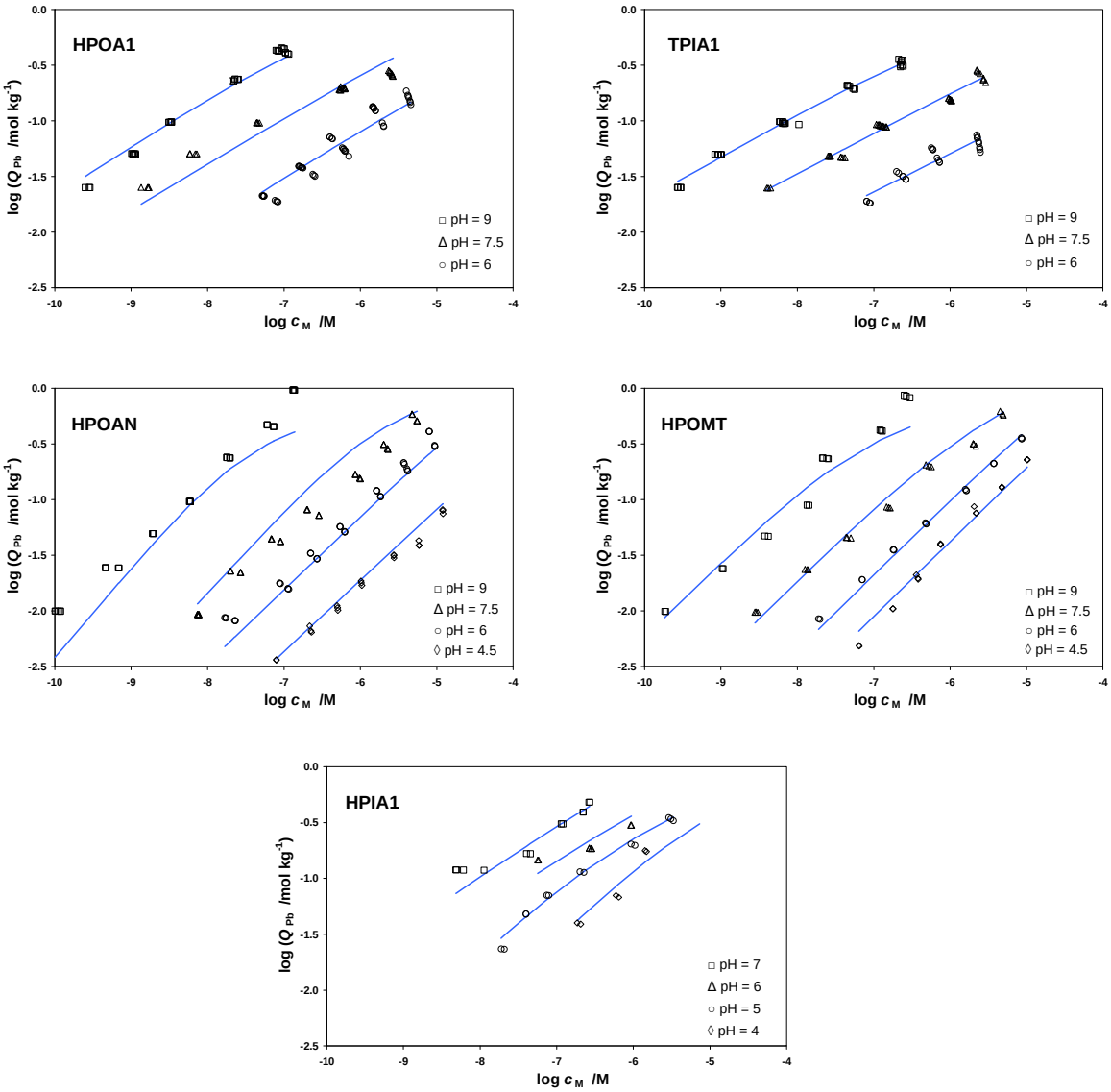

Fig 4: Pb binding to DOM fractions. Markers indicate experimental results from AGNES measurements, while the continuous lines stand for NICA fitting with parameters in Table 4.

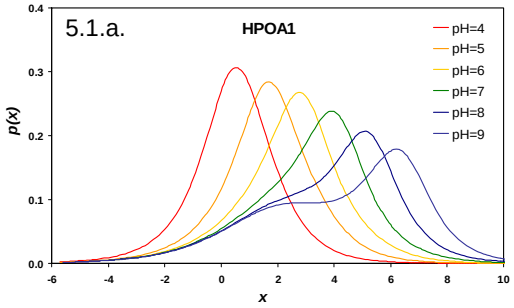
5.1.a.
HPOA1
pH=4
pH=5
pH=6
pH=7
pH=8
pH=9
p(x)
x

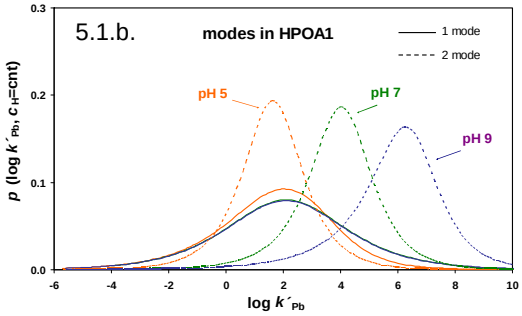
5.1.b.
modes in HPOA1
1 mode
2 mode
pH 5
pH 7
pH 9
p (log k´Pb, cH=cnt)
log k´Pb

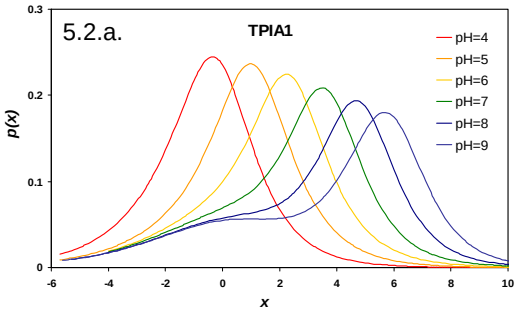
5.2.a.
TPIA1
pH=4
pH=5
pH=6
pH=7
pH=8
pH=9
p(x)
x

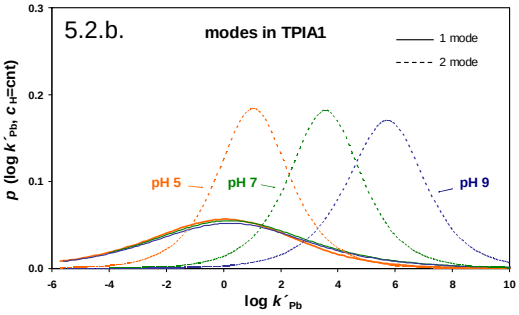
5.2.b.
modes in TPIA1
1 mode
2 mode
pH 5
pH 7
pH 9
p (log k´Pb, cH=cnt)
log k´Pb

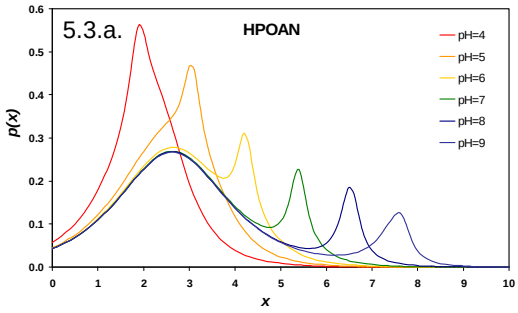
5.3.a.
HPOAN
pH=4
pH=5
pH=6
pH=7
pH=8
pH=9
p(x)
x

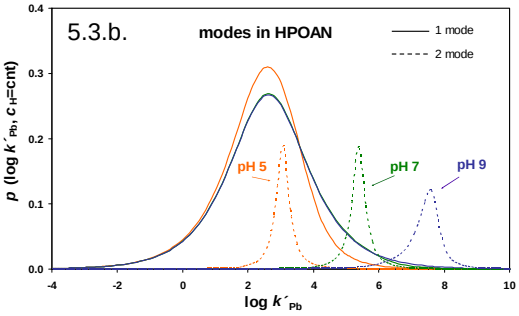
5.3.b.
modes in HPOAN
1 mode
2 mode
pH 5
pH 7
pH 9
p (log k´Pb, cH=cnt)
log k´Pb

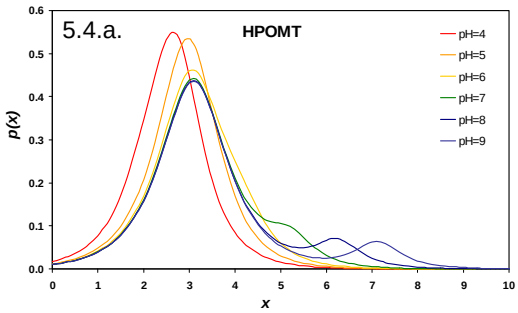
5.4.a.
HPOMT
pH=4
pH=5
pH=6
pH=7
pH=8
pH=9
p(x)
x

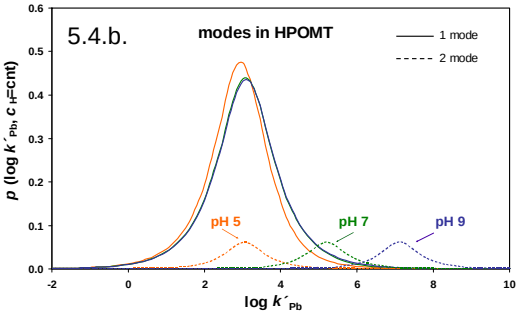
5.4.b.
modes in HPOMT
1 mode
2 mode
pH 5
pH 7
pH 9
p (log k´Pb, cH=cnt)
log k´Pb

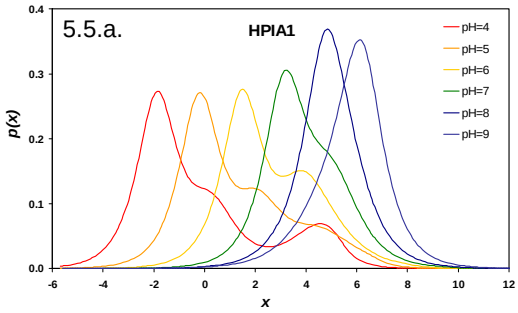
5.5.a.
HPIA1
pH=4
pH=5
pH=6
pH=7
pH=8
pH=9
p(x)
x

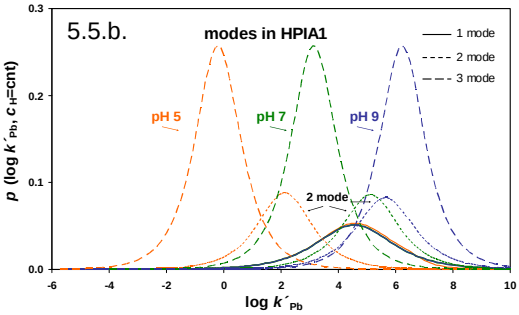
5.5.b.
modes in HPIA1
1 mode
2 mode
3 mode
pH 5
pH 7
pH 9
2 mode
p (log k´Pb, cH=cnt)
log k´Pb

Fig 5: Conditional Affinity Spectrum: full CAS (left column, panel “a”) and CAS for the elementary (e.g. phenolic and carboxylic) distributions (right column, panel “b”). Parameters taken from Tables 3 and 4

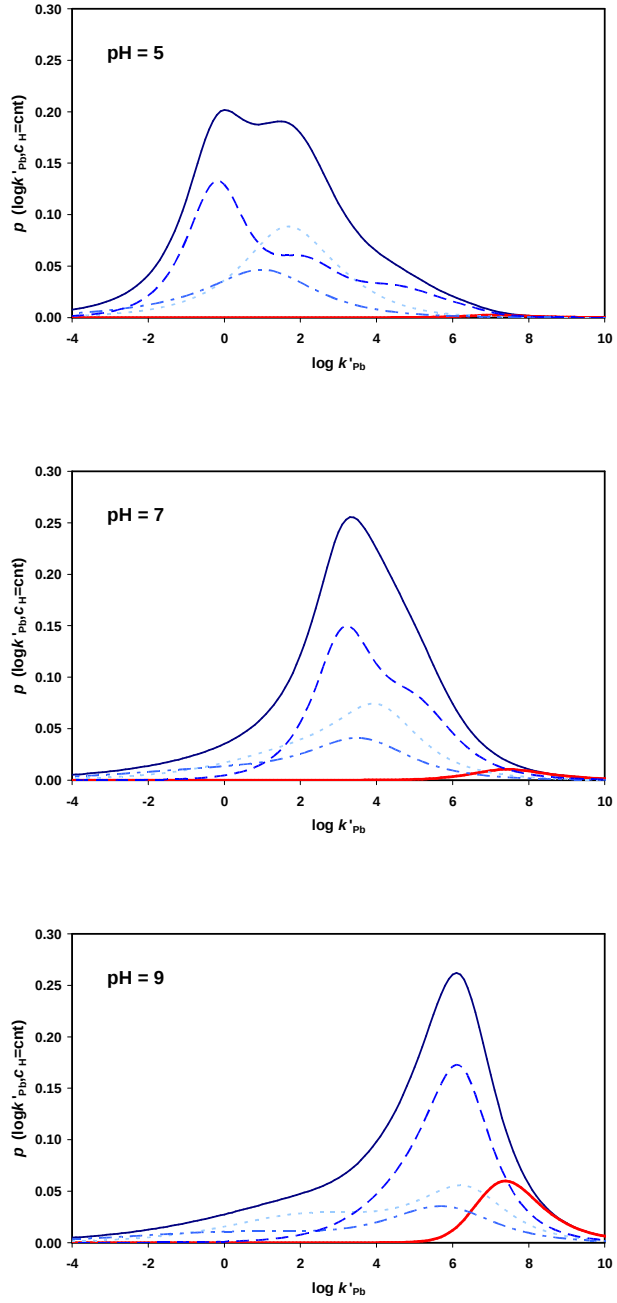

Figure 6 : Global CAS (continuous line) of the DOM in Achères sampling site obtained by the weighted addition of the CAS of the fractions HPOA1 (dotted line), TPIA1 (dotted dashed line) and HPIA1 (dashed line) at pH 5, 7 and 9. Lower (red) continuous line corresponds to the site occupation distribution function at a free Pb concentration of 10 $\mu g\ L^{-1}$.